Applied Science and Engineering Progress, Vol. 12, No. 1, pp. 44–51, 2019

Research Article

Selected Paper from the 6th International Thai Institute of Chemical Engineering and Applied Science Conference (ITIChE2016)

Low Temperature Corrosion: Oxidation of Carbon Steel and Stainless Steel in Air

Harich Krungkarnchana and Chutima Kongvarhodom*
Department of Chemical Engineering, Faculty of Engineering, King Mongkut's University of Technology Thonburi, Bangkok, Thailand

* Corresponding author. E-mail: chutima.kon@kmutt.ac.th DOI: 10.14416/j.ijast.2018.05.001
Received: 1 June 2017; Revised: 18 July 2017; Accepted: 31 July 2017; Published online: 17 May 2018

Abstract
An on-line corrosion monitor based on the principle of produced hydrogen effusion through a pipe wall due to the flow accelerated corrosion has been designed in an operating cycle mode which is complex. Using AISI 1045 and AISI 304 steels as material of probe equipped with this monitor expects to reduce the complexity of this system, the continuous mode. Type, characteristic and thickness of oxides formed on both steel surfaces affect the measurement of the rate of hydrogen production from the corrosion inside the pipe. Formation of oxides on AISI 1045 and AISI 304 at 673 K for 168 and 720 h in air was studied to determine type and thickness of oxides formed on steel surfaces under different exposure times. Oxidation of steels was performed in the heated air inside the furnace. The oxide formed on AISI 1045 surface was magnetite with different sizes of oxide particles because of the different exposure times. The oxide formed on AISI 304 surface was found as iron oxide and chromium oxide for 720 h. The thicknesses of oxides formed on AISI 1045 were 2.92 μm and 6.22 μm for 168 and 720 h, respectively. While the thicknesses of oxides formed on AISI 304 were not determined due to the irregular characteristic of oxide formed. Type and thickness of oxides obtained from this research could be used to predict the hydrogen pressure inside AISI 1045 and AISI 304 probes.

Keywords: Oxidation, Corrosion, Carbon steel, Stainless steel, Magnetite

1 Introduction

Corrosion of steel pipe is a serious problem causing wall thinning in many industries including power plants and petrochemical industries [1]–[4]. To prevent severe losses from corrosion, many devices have been created for monitoring the corrosion rate based on different operating principles. Steel pipes carrying high temperature and high pressure water are susceptible to wall thinning by Flow-Accelerated Corrosion (FAC). The flow accelerated corrosion produces the hydrogen atoms which effuse through the wall of steel pipe and form molecular hydrogen on the outer surface of the steel pipe [5]. One choice of devices to monitor the internal wall thinning rate is a Hydrogen Effusion Probe (HEP) by using the measured quantity of hydrogen effusing through the steel pipe leading to calculating the wall thinning rate [6]. This work has been developed by Centre for Nuclear Energy Research (CNER). Advantages of this hydrogen effusion probe are the online corrosion monitoring capability and the non-intrusive device. The disadvantage of the hydrogen effusion probe is a design to operate in a cyclic mode. After a predetermined pressure of 2,000 Pa is reached, the vacuum pump switches on to evacuate the volume and restart the cycle [7].

The initial material used for machining the hydrogen effusion probe is silver, a material of low hydrogen diffusivity and high corrosion resistance. The hydrogen effusion probe made by silver requires

Please cite this article as: H. Krungkarnchana and C. Kongvarhodom, "Low temperature corrosion: Oxidation of carbon steel and stainless steel in air," *Applied Science and Engineering Progress*, vol. 12, no. 1, pp. 44–51, Jan.–Mar. 2019.

a pump to vacuum the hydrogen gas inside the probe when the hydrogen pressure reaches the maximum value. This is because of the low hydrogen diffusivity of silver [5]. In this work, alternative materials such as AISI 1045 and AISI 304 are used for the hydrogen effusion probe which is expected to eliminate the cyclic mode and the vacuum pump because of the hydrogen permeation behavior of these metals [8], [9]. Also, the elimination of the pump results in less complicated equipment. AISI 1045 is a medium-carbon steel. It is used when greater strength, hardness and low cost steels are desired. AISI 304 is an austenitic stainless steel characterized by a comparatively low carbon content and, high chromium and nickel contents. It is particularly well suited for applications where welding is required and where the finished product must resist most severe forms of corrosion [10]. Moreover, carbon steel and stainless steel are a common steel grade and less expensive compared to silver [11], [12]. However, AISI 1045 and AISI 304 produce the oxide film in atmospheric air [13], [14]. The types of oxide layer formed on AISI 1045 surface are wustite, magnetite and hematite at 1,403 K [14]. For the type of oxide layer formed on AISI 304, it is chromium oxide with hematite at 1,073 K [12]. Both nickel and chromium in stainless steel, AISI 304, are the cause of a better oxidation resistance compared to AISI 1045 [15]. Oxide films formed on the steel surface are barriers for hydrogen diffusion affecting the diffusion of the atomic hydrogen through the wall of hydrogen effusion probe [6], [16]. However, the composition and thickness of the oxide film depending on temperature, time and material are needed to be considered under specific conditions [6], [12]–[14].

Oxidation is a chemical reaction between metal and oxygen. This reaction occurs naturally. The chemical reaction for the formation of oxide (M_aO_b) by oxidation between metal (M) and oxygen gas (O_2) can be written as:

$$aM + \frac{b}{2}O_2 \rightarrow M_aO_b \quad (1)$$

At the lower exposure time of oxidation, the oxidation rate follows the linear type of oxidation mechanism throughout the oxidation process. The initial step starts by the adsorption of oxygen on the clean metal surface during the metal-oxygen reaction. This behavior is a result of the controlling mechanism

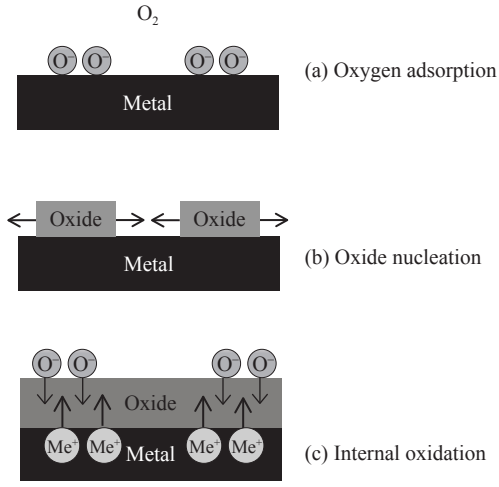

Figure 1: Scale formation during high temperature metal oxidation: (a) oxygen adsorption, (b) oxide nucleation and (c) thin oxide film formation (This figure was reproduced from [17]).

of oxidation. Since the oxide layer is very thin providing no significant resistance to the transport of oxygen ion for the oxidation on steel surface, the rate of the chemical reaction at the steel surface is controlled resulting in a linear behavior. After the longer time of oxidation, the oxide layer reaches an effective thickness. At this thickness, the oxidation process is controlled by the solid state diffusion of the oxygen ion through the oxide layer as shown in Figure 1 [17], [18].

However, the information of the formation of oxides on carbon steel and stainless steel at low temperature is scarce. The purpose of this research is, therefore, to investigate the effects of materials and exposure times on the formation of oxides on steel surfaces at low temperature. The obtained results can be used to predict the formation of oxide films on the steel leading to estimate the hydrogen pressure in the HEP resulting from the hydrogen diffusion through the pipe wall into the HEP caused by corrosion. This research includes the determination of the types of oxide formed on the steel samples and characterization of these oxide films. The rate of oxide formation on the steel surface was also determined from the weight gain of the samples and the thicknesses of oxide formed on the steel samples were measured from the cross-sectional images obtained by a Scanning Electron Microscope (SEM).

2 Methodology

Both of AISI 1045 and AISI 304 samples were cut into 20 mm in diameter with a thickness of 2 mm. AISI 1045 carbon steel contains 0.43–0.50 wt% C, 0.04 wt% P, 0.05 wt% S and 0.60–0.90 wt% Mn. AISI 304 stainless steel contains 0.08 wt% C, 0.045 wt% P, 0.03 wt% S, 1.00 wt% Si, 2.0 wt% Mn, 18–20 wt% Cr and 8.0–10.5 wt% Ni [10]. The main difference in chemical compositions between AISI 1045 and AISI 304 is Cr and Ni. The AISI 1045 and AISI 304 samples were abraded with silicon carbide abrasive papers from no. 60, 120, 240, 400, 600, 800, 1200 and 4000, rinsed with acetone and dried. Oxidation of the samples was performed in heated air inside a furnace for 168 and 720 h at 673 K. The samples were suspended from an aluminium wire in the furnace and exposed to hot air. After oxidation process was completed, the samples were kept in a desiccator to cool down to room temperature before the characterization of oxidized samples.

The microstructures and cross-sectional images of all oxidized samples were analysed by a JEOL JSM-6610 Scanning Electron Microscope (SEM). The chemical compositions of oxide formed on samples were analysed by a scanning electron microscope equipped with an Oxford INCA350 Energy Dispersive Spectroscopy (EDS). Types of oxide on surface samples were analysed by a BRUKER D8 DISCOVER X-ray Diffractometer (XRD).

3 Results and Discussion

3.1 *Characterization of the oxide formed on steel surfaces*

The fresh polished AISI 1045 and AISI 304 samples were analysed by SEM, EDS and XRD before the oxidation to obtain baseline data for each metal. Both of AISI 1045 and AISI 304 samples were mechanically polished to smooth surfaces. SEM images of AISI 1045 surfaces after exposure to air at 673 K for 168 and 720 h are shown in Figures 2 and 3. The oxide was distributed uniformly with different sizes of flakes due to the different exposure times. The longer exposure time provided the bigger size of the flakes. This is because the longer exposure time allows more oxygen ions diffusing through oxide films, hence, more oxidation of steel [6].

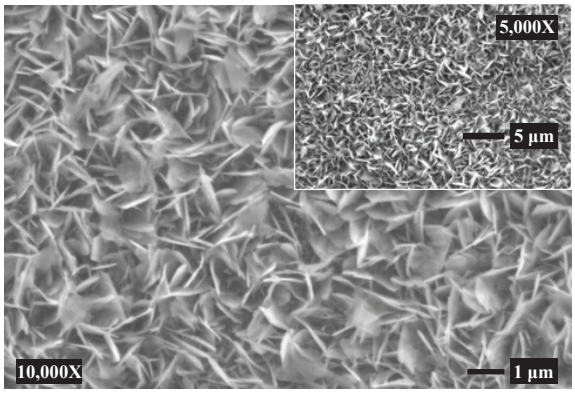

Figure 2: SEM images after exposure to 673 K of AISI 1045 for 168 h.

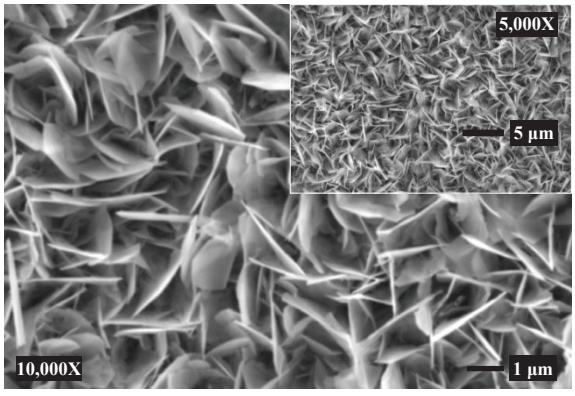

Figure 3: SEM images after exposure to 673 K of AISI 1045 for 720 h.

The SEM images, Figures 4 and 5, show the distribution of oxide particles on the surfaces of AISI 304 after exposure to air at 673 K for 168 and 720 h. The oxide film was barely observed obviously at 168 h because oxide particles were very small. However, the oxide formation was confirmed with EDS result. While the irregular oxide particles could be seen in some locations for 720 h.

The oxygen contents were not appeared in EDS results of the fresh polished AISI 1045 and AISI 304 samples. This indicates that the oxides were not formed on the fresh samples before oxidation. The EDS results as shown in Figure 6 show that the atomic percentages of oxygen of oxidized AISI 1045 for 168 and 720 h were 57.77 and 56.77, respectively.

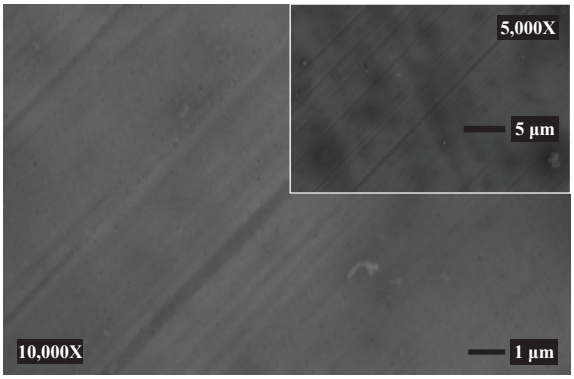

Figure 4: SEM images after exposure to 673 K of AISI 304 for 168 h.

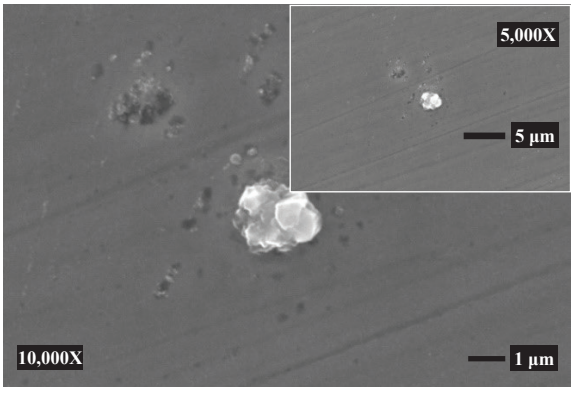

Figure 5: SEM images after exposure to 673 K of AISI 304 for 720 h.

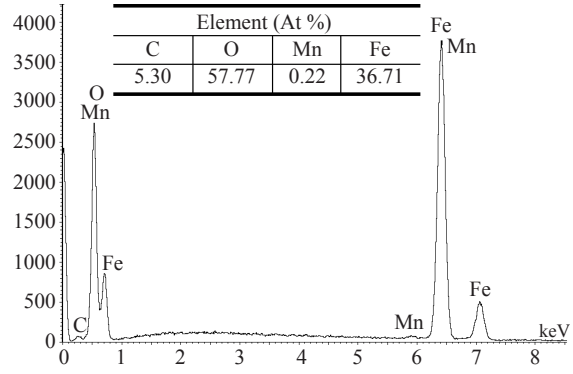

(a) 168 h

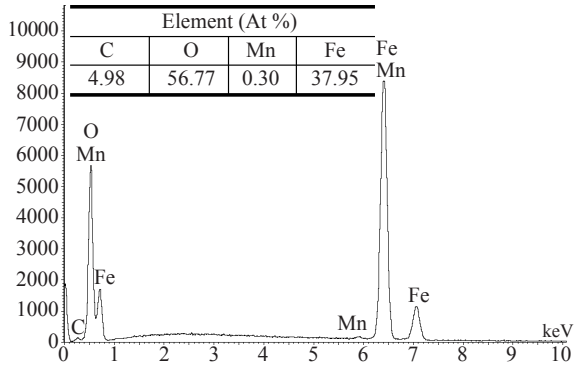

(b) 720 h

Figure 6: EDS results of AISI 1045 after exposure to 673 K for (a) 168 h and (b) 720 h.

The atomic percentages of oxygen of oxidized AISI 304 for 168 and 720 h as shown in Figure 7 were found to be 4.03 and 8.11, respectively. This indicates that the oxygen was adsorbed on the surfaces. The SEM images of oxidized AISI 304 surfaces did not show the oxide particles for 168 h because the chromium addition in steels provided resistance to corrosion and scaling [10]. Therefore, the oxide formation was retarded so that the oxide particles were too small to be visualised. For 720 h, the particle formed on AISI 304 as shown in Figure 5 was also analysed by EDS, Figure 8. The EDS result on this particle shows that the atomic percentage of oxygen was 55.39, atomic percentage of iron was 21.80, atomic percentage of chromium was 8.01 and atomic percentage less than 7 for each of carbon, silicon, manganese, sulfur and nickel. Therefore, the particle might be iron oxide and/or chromium oxide.

The XRD spectra in Figure 9, show that the oxides on AISI 1045 surfaces were magnetite (Fe_3O_4) for 168 and 720 h. However, the peak of the magnetite was not found on bare steel indicating no oxide on the steel samples before the oxidation process. The apparently 2Θ of the magnetite peaks were found at 35.43º, 56.94º and 62.93º. The higher detected peaks on the XRD indicate the presence of highly pure and crystalline oxide showing the relative amount of each phase which is proportional to the integrated intensity under the corresponding pattern [19]. However, no peak of oxides on AISI 304 surfaces for 168 and 720 h was appeared in XRD spectra as shown in Figure 10. The peaks of iron, nickel and chromium were found as they are constituents in stainless steel. The detection limit of XRD is reported to be 5 vol% of oxides. This could be the reason why the peak of oxide was not observable.

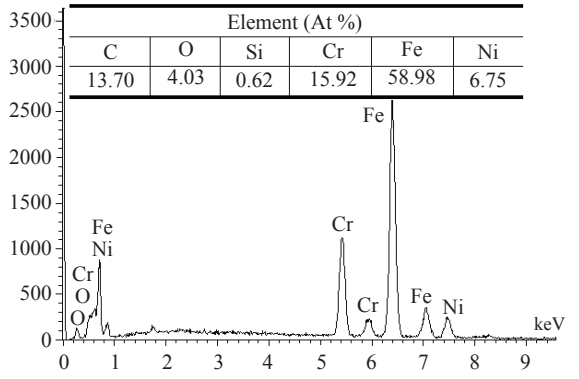

(a) 168 h

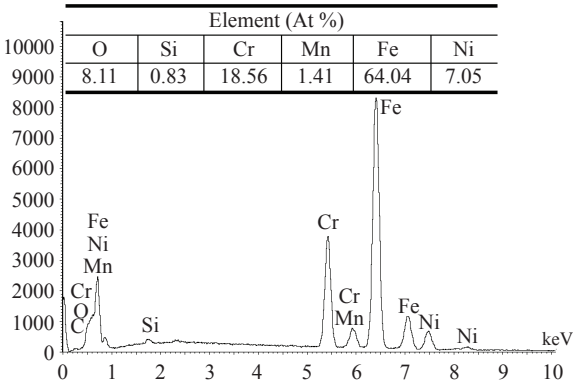

(b) 720 h

Figure 7: EDS results of AISI 304 after exposure to 673 K for (a) 168 h and (b) 720 h.

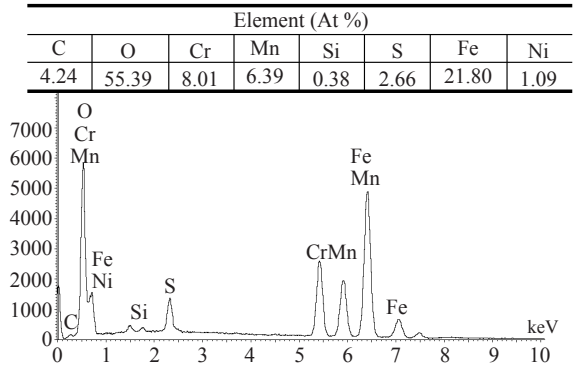

Figure 8: EDS result of irregular oxide particles on AISI 304 surface shown in Figure 5 after exposure to 673 K for 720 h.

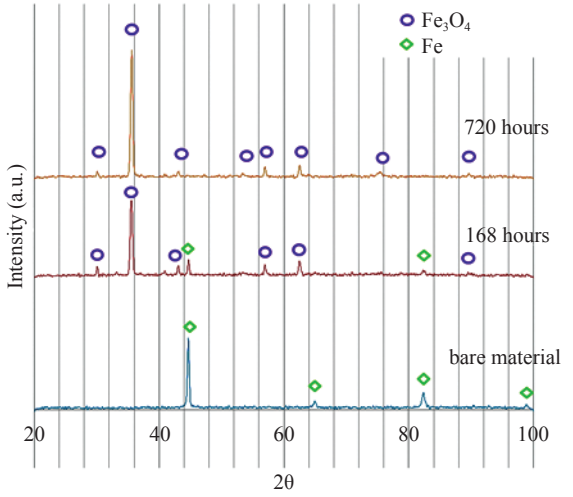

Figure 9: XRD spectra of AISI 1045 oxidized for 168 and 720 h at 673 K.

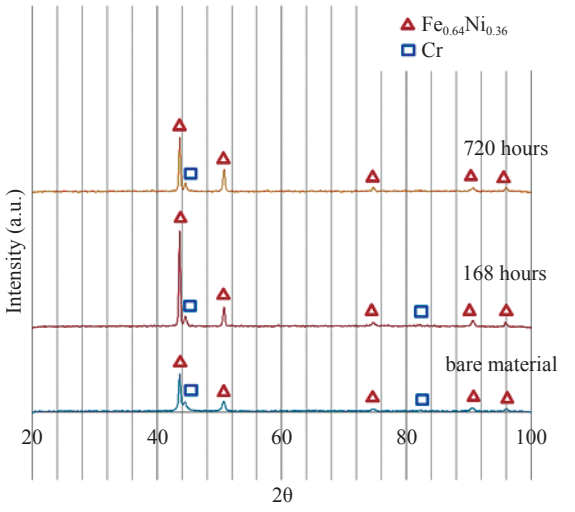

Figure 10: XRD spectra of AISI 304 oxidized for 168 and 720 h at 673 K.

3.2 *Weight gain of samples and thickness of oxide layers*

The weight gain per unit area of each steel sample is shown in Figure 11. Weight gain per unit area of both materials increased with exposure time. The weight gain per unit area obtained from the oxidation of AISI 1045 in air was much higher than

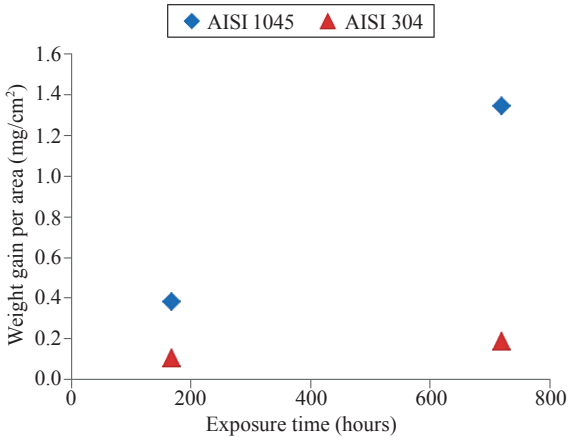

Figure 11: Relation between the weight gain per unit area and exposure time at 673 K.

that of AISI 304 because of chromium and nickel components in AISI 304. Both nickel and chromium in stainless steel provide a better oxidation resistance because of the small pore of oxide layer on stainless steel containing high chromium or nickel content [15], only allowing small amount of oxygen ions diffusing to AISI 304 surface.

However, the thicknesses of oxides formed on AISI 1045 and AISI 304 could not be determined from the weight-gain measurement because the oxides formed on surfaces were porous and not uniform. Furthermore, the weight-gain data account for all oxygen atoms adsorbed in steels but some adsorbed oxygen atoms may not form oxide on steel surfaces. Therefore, the oxide thickness was obtained from the cross-sectional image. All oxide thickness measurements were performed on the SEM images under the same magnification. The same number of measurements was also done on each image at consistent location. Figures 12 and 13 represent the oxide thickness measurements on AISI 1045 samples which were oxidized at 673 K for 168 and 720 h. The thicknesses of oxides formed on AISI 1045 for 168 and 720 h with SEM cross-sectional images were found to be 2.92 µm and 6.22 µm, respectively.

Based on the data of SEM cross-sectional images, the change in oxide thickness with time of AISI 1045 for 720 h is lower than that of AISI 1045 for 168 h because the thicker oxide layers formed on the AISI 1045 surface for 720 h act as the barrier retarding oxygen diffusion to the iron/metal interface [6].

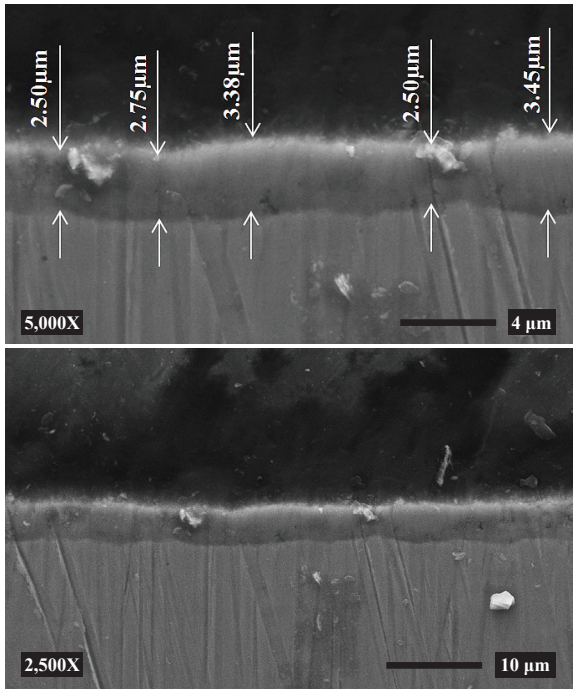

Figure 12: SEM cross-sectional images after exposure to 673 K of AISI 1045 for 168 h.

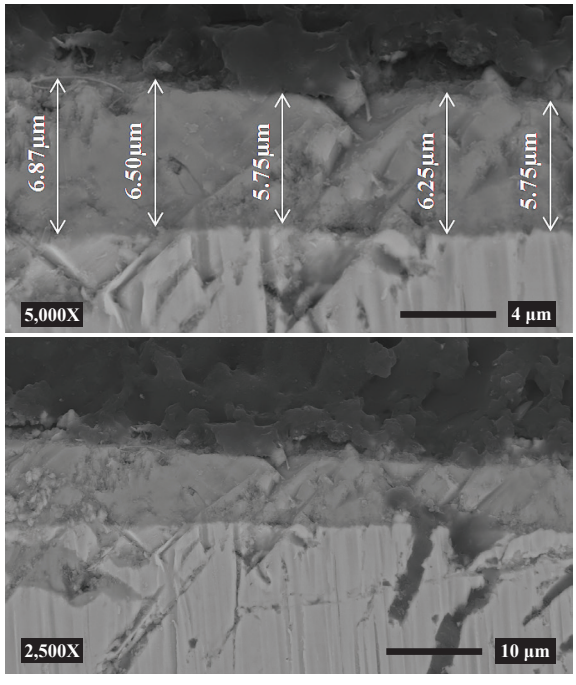

Figure 13: SEM cross-sectional images after exposure to 673 K of AISI 1045 for 720 h.

3.3 *Model of hydrogen diffusion through oxide layer formed on steel surface*

Hydrogen inside the instrument, HEP, could transport through the wall of instrument made of carbon steel or stainless steel including the oxide layer formed on these steel instruments into the atmosphere driven by hydrogen concentration gradient [20]. The instrument wall incorporated with the oxide layer acts as a diffusion resistance to reduce the rate of hydrogen effusion to the atmosphere. Thus, the hydrogen diffusion resistance includes a hydrogen diffusion resistance through the oxide layer and a hydrogen diffusion resistance through the instrument wall. These hydrogen diffusion resistances depend on the instrument wall thickness, the oxide layer thickness, the hydrogen diffusion coefficient of oxide and the hydrogen diffusion coefficient of instrument material as shown in Equations (2) and (3).

$$R_{ox} = \frac{x}{D_{H_2,\,oxide\ layer}} \tag{2}$$

$$R_{w} = \frac{\delta}{D_{H_2,\,wall}} \tag{3}$$

R_{ox} is hydrogen diffusion resistance through the oxide layer (s/m), R_w is hydrogen diffusion resistance through the instrument wall (s/m), x is oxide thickness (m), δ is instrument wall thickness (m), $D_{H_2,oxide\ layer}$ is hydrogen diffusion coefficient through oxide layer (m^2/s) and $D_{H_2,wall}$ is hydrogen diffusion coefficient through instrument wall (m^2/s). The hydrogen diffusion coefficients through AISI 1045 and AISI 304 [8], [21] indicate that the hydrogen diffusion resistance through AISI 1045 instrument wall is less than that of AISI 304 instrument wall. However, the oxide layer obtained from the oxidation of AISI 1045 in air in this research can be seen obviously compared to the oxide formed on AISI 304 surface under the same condition leading to the higher hydrogen diffusion resistance through the AISI 1045 surface with the oxide layer.

These hydrogen diffusion resistances can be applied to the model of hydrogen diffusion through oxide layer formed on steel surface in order to determine the amount of hydrogen diffusion through the instrument wall, Equation (4). This leads to identifying the amount of hydrogen pressure inside the instrument (HEP) and the corrosion rate depending on the pipe wall thickness and the hydrogen diffusion coefficient through pipe wall on which the instrument would be installed.

$$J_{H_2}^{HEP} = \frac{C_{H_2}^{inside} - C_{H_2}^{outside}}{R_{ox} + R_w} \tag{4}$$

$J_{H_2}^{HEP}$ is hydrogen flux through instrument wall (mol/s·m^2), $C_{H_2}^{inside}$ is concentration of hydrogen inside the instrument (mol/m^3) and $C_{H_2}^{outside}$ is concentration of hydrogen outside the instrument (mol/m^3).

4 Conclusions

The oxides formed on the AISI 1045 surfaces exposed to air at 673 K for 168 and 720 h were magnetite which was in flake form of different sizes. The longer exposure time provided the bigger size of the flakes. The oxides formed on AISI 304 surfaces for 673 K could be iron oxide and/or chromium oxide. The oxidation rate of AISI 304 was much lower than that of AISI 1045. The results of oxide formation on AISI 1045 and AISI 304 obtained from this work lead to determining the hydrogen diffusion resistance through the instrument wall incorporated with the oxide layer. The calculated resistance can be used to predict the amount of hydrogen pressure inside the instrument (HEP) and the corrosion rate relating to hydrogen evolution during corrosion. The calculation is based on the principle that one mole of hydrogen gas is produced for one mole of iron loss [6]. The air-formed oxides on the AISI 1045 surfaces acted as a barrier for hydrogen diffusion affecting the diffusion of the atomic hydrogen through the wall of hydrogen effusion probe [6], [16]. Therefore, AISI 304 would be more appropriate for HEP application at high temperature.

Acknowledgements

The authors acknowledge financial support from King Mongkut's University of Technology Thonburi Research Fund 2015. The authors would like to convey special appreciation to the academic committee of The 6th International Thai Institute of Chemical Engineering and Applied Science Conference (ITIChE 2016) for providing the opportunity for this work to be published in this journal.

References

[1] M. G. Fontana, *Corrosion Engineering*, 3rd ed. New York: McGraw-Hill Book Company, 1986.

[2] M. Imran, "Effect of corrosion on heat transfer through boiler tube and estimating overheating," *International Journal of Advanced Mechanical Engineering*, vol. 4, pp. 629–638, 2014.

[3] V. Chawla, A. Chawla, D. Puri, S. Prakash, P. G. Gurbuxani, and B. S. Sidhu, "Hot corrosion & erosion problems in coal based power plants in India and possible solutions," *Journal of Minerals & Materials Characterization & Engineering*, vol. 10, no. 4, pp. 367–385, 2011.

[4] F. Nasirpouri, A. Mostafaei, L. Fathyunes, and J. Robabeh, "Assessment of localized corrosion in carbon steel tube-grade AISI 1045 used in output oil–gas separator vessel of desalination unit in oil refinery industry," *Engineering Failure Analysis*, vol. 40, pp. 75–88, 2014.

[5] A. John, "Device and system for corrosion detection," U.S. Patent 7552643, Jun. 3, 2009.

[6] S. Weerakul, F. R. Steward, T. Rirksomboon, A. Feicht, and C. Kongvarhodom, "Kinetics of oxide formation on carbon steel surface in the presence of oxygen nitrogen mixtures," *Chemical Engineering Transactions*, vol. 29, pp. 973–978, 2012.

[7] K. McKeen, M. Lalonde, A. Scott, and J. Ross, "Hydrogen effusion probe development and installation at the point lepreau nuclear generating station," presented at the 28th Annual Canadian Nuclear Society Conference, Canada, Jun. 3–6, 2007.

[8] W. M. Robertson and A. W. Thompson, "Permeation measurements of hydrogen trapping in 1045 steel," *Metallurgical Transactions A*, vol. 11A, pp. 553–557, 1980.

[9] H. G. Nelson and J. E. Stein, "Gas-phase hydrogen permeation through alpla iron, 4310 steel, and 304 stainless steel from less than 1,000ºC to near 6,000ºC," National Aeronautics and Space Administration, Washington, DC, Rep. A-4749, Apr. 1973.

[10] P. D. Harvey, *Engineering Properties of Steel*, 5th ed. Geauga, OH: American Society for Metals, 1995.

[11] H. S. Joo, S. K. Hwang, H. M. Baek, Y. T. Im, I. H. Son, and C. M. Bae, "Manufacturing of medium carbon steel wires with improved spheroidization by non-circular drawing sequence," *Procedia Engineering*, vol. 81, pp. 682–687, 2014.

[12] P. Horodek, K. Siemek, A. G. Kobets, M. Kulik, and I. N. Meshkov, "Positron beam and RBS studies of thermally grown oxide films on stainless steel grade 304," *Applied Surface Science*, vol. 333, pp. 96–103, 2015.

[13] L. Jinlong, L. Hongyun, L. Tongxian, and G. Wenli, "The effects of grain refinement and deformation on corrosion resistance of passive film formed on the surface of 304 stainless steels," *Materials Research Bulletin*, vol. 70, pp. 896–907, 2015.

[14] N. Yukawa, Y. Nakashima, T. Ishiguro, E. Abe, T. Ishikawa, and T. Choda, "Modeling of heat transfer coefficient of oxide scale in hot forging," *Procedia Engineering*, vol. 81, pp. 492–497, 2014.

[15] O. Srihakulung, "Effect of chromium and nickel addition in 316L stainless steel produced by casting on microstructure and oxidation resistance," M.S. thesis, Faculty of Engineering, Chulalongkorn University, Bangkok, 2013 (in Thai).

[16] S.-I. Pyun and R. A. Oriani, "The permeation of hydrogen through the passivating films on iron and nickel," *Corrosion Science*, vol. 29, no. 5, pp. 485–496, 1988.

[17] A. K. M. Nural Amin, *Titanium Alloys - Towards Achieving Enhanced Properties for Diversified Applications*. Rijeka, Croatia: InTech, 2012.

[18] D. Talbot and J. Talbot, *Corrosion Science and Technology*. Boca Raton, Florida: CRC Press, 1997.

[19] R. Montanari, "High-temperature XRD investigations on phase transformations," *La Metallurgia Italiana*, pp. 23–30, 2004.

[20] Y. F. Cheng and F. R. Steward, "Corrosion of carbon steels in high-temperature water studied by electrochemical techniques," *Corrosion Science*, vol. 46, pp. 2405–2420, 2004.

[21] D. M. Grant, D. L. Cummings, and D. A. Blackburn, "Hydrogen in 304 steel: Diffusion, permeation and surface reaction," *Journal of Nuclear Materials*, vol. 149, no. 2, pp. 180–191, 1987.